THE JOURNAL OF PHYSICAL CHEMISTRY LETTERS
A JOURNAL OF THE AMERICAN CHEMICAL SOCIETY

pubs.acs.org/JPCL

Letter

Simulating Polaritonic Ground States on Noisy Quantum Devices

Mohammad Hassan, Fabijan Pavošević,* Derek S. Wang, and Johannes Flick*

Cite This: *J. Phys. Chem. Lett.* 2024, 15, 1373−1381

Read Online

ACCESS | Metrics & More | Article Recommendations | Supporting Information

ABSTRACT: The recent advent of quantum algorithms for noisy quantum devices offers a new route toward simulating strong light−matter interactions of molecules in optical cavities for polaritonic chemistry. In this work, we introduce a general framework for simulating electron−photon-coupled systems on small, noisy quantum devices. This method is based on the variational quantum eigensolver (VQE) with the polaritonic unitary coupled cluster (PUCC) ansatz. To achieve chemical accuracy, we exploit various symmetries in qubit reduction methods, such as electron−photon parity, and use recently developed error mitigation schemes, such as the reference zero-noise extrapolation method. We explore the robustness of the VQE-PUCC approach across a diverse set of regimes for the bond length, cavity frequency, and coupling strength of the H_2 molecule in an optical cavity. To quantify the performance, we measure two properties: ground-state energy, fundamentally relevant to chemical reactivity, and photon number, an experimentally accessible general indicator of electron−photon correlation.

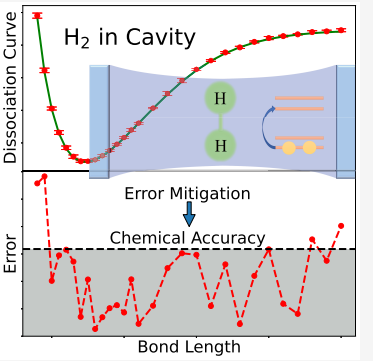

Polaritonic chemistry is a field that exploits strong light−matter interactions for manipulating chemical reactions.[1−7] These strong light−matter interactions can be created inside micro/nano/picocavities[8−10] where the light field strongly couples with a molecular system, giving rise to hybrid light−matter states known as molecular polaritons. By tuning the light field strength inside a cavity, a molecular reaction can then be selectively and noninvasively modified.[11−13]

These experimental advances have been accompanied by the development of theoretical methods that can offer insights into the fundamental principles that govern polariton-assisted chemical transformations. Among the various theoretical approaches,[5,7,14−18] a particularly robust class is the quantum electrodynamics (QED) *ab initio* methods, such as quantum electrodynamics density functional theory (QED-DFT)[19−22] and quantum electrodynamics coupled cluster methods (QED-CC),[23−27] in which both electrons and photons are treated quantum mechanically. Although these methods have provided significant insight into chemical reactions inside a cavity,[22,24,28−30] practical implementations of these methods rely on numerous approximations limiting their applicability to weakly correlated molecular systems. Therefore, these methods are expected to fail in the correct description of strongly correlated systems which play a crucial role in transition metal chemistry, photochemistry, catalysis, and bond-breaking processes,[31] among others. Strongly correlated systems can be accurately described with multireference quantum chemistry methods where the corresponding wave function is expanded in terms of excited electronic configurations.[32] However, because the number of these configurations scales factorially with the system size, multireference methods are currently unsuitable for simulating large molecules.

Quantum algorithms offer an alternative way for solving complex chemical problems.[33−35] One such quantum algorithm for solving the electronic structure problem is the quantum phase estimation (QPE) algorithm.[36] Although the QPE algorithm offers an exponential speedup for the evaluation of eigenvalues of the molecular Hamiltonian over its classical counterparts, it requires very deep circuits composed of millions of quantum gates.[37] Therefore, this algorithm exceeds the capacity of currently available noisy quantum devices.[38]

An alternative to the QPE algorithm that is more suitable for noisy quantum devices is an iterative hybrid quantum-classical algorithm: the variational quantum eigensolver (VQE).[39] In the VQE, the quantum device is utilized for the classically intractable parts of computations, such as the quantum-state preparation and the ground-state energy measurement, whereas the classical computer is employed for the optimization of the parameters that minimize the ground-state energy. By outsourcing the optimization routine to a classical computer, the VQE algorithm exhibits more modest quantum requirements than the QPE algorithm. The VQE algorithm has been successfully implemented on different noisy quantum devices for simulation of molecular systems, including trapped ion devices,[40,41] photonic quantum processors,[39] and superconducting qubits.[42−44]

Received: October 13, 2023
Revised: January 5, 2024
Accepted: January 9, 2024
Published: January 29, 2024

In practice, the quality of the VQE result depends on the choice of the parametrized wave function ansatz. In its first implementation, the VQE algorithm employed the unitary coupled cluster with singles and doubles (UCCSD) ansatz.[39] The advantages of the UCCSD ansatz are that it is unitary, variational, systematically improvable, and performant for the simulation of strongly correlated systems, in particular for bond-breaking processes.[42] However, because the UCCSD ansatz results in deep quantum circuits along with a large number of wave function parameters, practical implementations of this method on quantum devices require careful optimization of the algorithm, such as term truncation, to minimize quantum resources.

Encouraged by the success of the VQE algorithm for molecular simulations on noisy quantum devices, as well as by the need for a robust method for simulation of strongly correlated systems confined to a cavity, we have previously developed an ansatz referred to as the quantum electrodynamics unitary coupled cluster with singles and doubles (QED-UCCSD).[25] Therein, we have demonstrated that the QED-UCCSD ansatz for VQE is in excellent agreement with the exact method, even in the regions of the potential energy surface where the strong electronic correlations become significant. In the remainder of this work, we will refer to the QED-UCCSD ansatz as the polaritonic unitary coupled cluster (PUCC) ansatz, and VQE-PUCC will refer to the method of using the VQE with the PUCC ansatz.

In this work, we study the VQE-PUCC method using realistic noise models and leverage physical symmetries and composite error mitigation strategies to improve the results. The main motivation for this work is to present the formalism, working equations, and technical details for the efficient use of quantum devices to simulate systems where electrons and photons are strongly coupled. Among these technical details is the deployment of appropriate error mitigation techniques to precisely resolve ground-state observables, such as the ground-state energies and photon numbers, even in coupling regimes where differences are small. Overall, these results demonstrate the practical feasibility of quantum simulations of mixed fermion−boson systems, such as molecular polaritons, on noisy quantum hardware.

The interaction of an embedded molecular system inside an optical cavity and the quantized light field can be described by the Pauli−Fierz Hamiltonian.[2] This Hamiltonian—within the dipole approximation and in the coherent-state basis[23] for a single-mode cavity in second quantization notation—reads as

$$\hat{H} = h_q^p a_p^q + \frac{1}{4}\overline{g}_{rs}^{pq} a_{pq}^{rs} + \omega b^\dagger b - \sqrt{\frac{\omega}{2}}(\boldsymbol{\lambda}\cdot\Delta\boldsymbol{d})(b^\dagger + b) + \frac{1}{2}(\boldsymbol{\lambda}\cdot\Delta\boldsymbol{d})^2 \tag{1}$$

The first two terms in this equation correspond to the electronic Born−Oppenheimer Hamiltonian (note that extensions to include nonadiabatic effects are also possible[45−47]), where $a_{p_1p_2\ldots p_n}^{q_1q_2\ldots q_n} = a_{q_1}^\dagger a_{q_2}^\dagger \ldots a_{q_n}^\dagger a_{p_n}\ldots a_{p_2}a_{p_1}$ are the second-quantized electronic excitation operators expressed in terms of fermionic creation ($a^\dagger$) and annihilation (a) operators. Additionally, $h_q^p = \langle q|\hat{h}|p\rangle$ is a matrix element of the one-electron core Hamiltonian and $\overline{g}_{rs}^{pq} = g_{rs}^{pq} - g_{rs}^{qp} = \langle rs|pq\rangle - \langle rs|qp\rangle$ is the antisymmetrized two-electron Coulomb repulsion tensor element. Furthermore, p, q, r, s, ... indices denote general electronic spin−orbitals, i, j, k, l, ... indices denote occupied electronic spin−orbitals, and a, b, c, d, ... indices denote unoccupied (virtual) electronic spin−orbitals. The third term of eq 1 represents the Hamiltonian of the cavity photon mode with frequency ω. There, operators $b^\dagger$ and b are bosonic creation and annihilation operators, respectively. The fourth term accounts for the interactions of electronic and photonic degrees of freedom. Finally, the last term corresponds to the dipole self-energy. Within the last two terms, $\boldsymbol{\lambda} = (\lambda_x, \lambda_y, \lambda_z)$ with $\lambda = |\boldsymbol{\lambda}|$ is the coupling strength vector and $\Delta\boldsymbol{d} = \boldsymbol{d} - \langle\boldsymbol{d}\rangle$ is the total molecular dipole moment operator subtracted by its expectation value that arises due to the coherent-state basis transformation.[23] Note that the total molecular dipole moment is defined as $\boldsymbol{d} = \boldsymbol{d}_{\text{electronic}} + \boldsymbol{d}_{\text{nuclear}}$.

Within the VQE algorithm, the ground-state energy of a system inside a cavity (E_{QED}) is determined by variationally minimizing the energy functional

$$E_{\text{QED}} = \min_{\theta_{\mu,n}} \langle\Psi_{\text{QED}}(\theta_{\mu,n})|\hat{H}|\Psi_{\text{QED}}(\theta_{\mu,n})\rangle \tag{2}$$

with respect to wave function parameters $\theta_{\mu,n}$. In this equation, $|\Psi_{\text{QED}}(\theta_{\mu,n})\rangle$ is the trial wave function that depends on parameters $\theta_{\mu,n}$. In the case of the PUCC method, the wave function is defined as

$$|\Psi_{\text{PUCC}}\rangle = e^{\hat{T}-\hat{T}^\dagger}|0^e0^{ph}\rangle \tag{3}$$

where $|0^e0^{ph}\rangle = |0^e\rangle\otimes|0^{ph}\rangle$ corresponds to the reference quantum electrodynamics Hartree−Fock (QED-HF) wave function[23] defined in terms of an electronic Slater determinant ($|0^e\rangle$) and a zero-photon state ($|0^{ph}\rangle$). Because the interaction of the quantum particles (i.e., electrons and photons) is accounted for through a mean-field potential, correlation effects are not included in the QED-HF method. In eq 3, $\hat{T}$ is the cluster operator

$$\hat{T} = \sum_{\mu,n} \theta_{\mu,n} a^\mu (b^\dagger)^n \tag{4}$$

where $a^\mu = a_\mu^\dagger = \{a_i^a, a_{ij}^{ab}, \ldots\}$ is a set of single, double, and higher electronic excitation operators, μ is an excitation manifold, and n is the number of photons. Therefore, action of the operator $a^\mu(b^\dagger)^n$ on the QED-HF reference will produce the excited configuration

$$a^\mu(b^\dagger)^n|0^e0^{ph}\rangle = \sqrt{n!}\,|\mu\rangle \otimes |n\rangle \tag{5}$$

that accounts for the correlation effects between quantum particles. Because of the unitary form of the wave function,[25] the PUCC method is suitable for quantum computations, since quantum computers implement unitary operators via quantum gates.[33−35,39,48] Truncation of the excitation cluster operator up to a certain electronic excitation manifold and the number of photons establishes the systematically improvable PUCC hierarchy. In cases where the electronic excitation rank equals the number of electrons, the method is said to be exact. In this work, we consider the truncated cluster operator defined as

$$\hat{T} = \theta_a^{i,0} a_i^a + \theta^{0,1} b^\dagger + \frac{1}{4}\theta_{ab}^{ij,0} a_{ij}^{ab} + \theta_a^{i,1} a_i^a b^\dagger + \frac{1}{4}\theta_{ab}^{ij,1} a_{ij}^{ab} b^\dagger \tag{6}$$

where up to one photon and up to two electrons interact with each other.[23] In the original proposal, this method was coined as QED-UCCSD-1.[25] Importantly, the QED-UCCSD-1 method is exact for systems comprising two electrons interacting with at most one photon. One such system that

https://doi.org/10.1021/acs.jpclett.3c02875
J. Phys. Chem. Lett. 2024, 15, 1373−1381

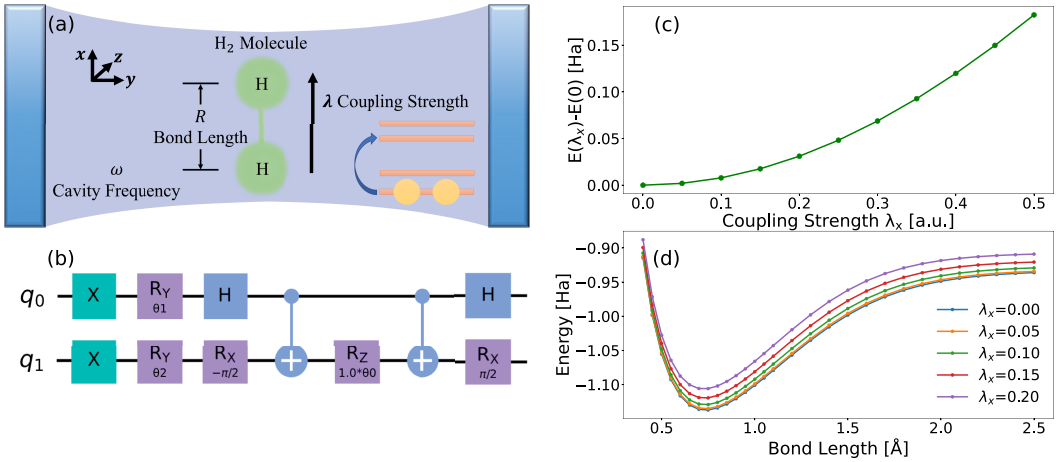

Figure 1. (a) Schematic of an H_2 molecule in an optical cavity. A cavity mode of frequency ω interacts with the electronic system of H_2 with bond length R via electron−photon coupling strength λ. (b) The reduced ansatz circuit obtained by using Bravyi−Kitaev mapping and tapering off a qubit using $\mathcal{Z}_2$ symmetries. (c) and (d) show FCI calculations for H_2 interacting with a single photon mode. (c) The energy difference of the system between the coupling strength λ_x and $\lambda = 0$ a.u. ($\omega = 2$ eV, $R_0 = 0.735$ Å). (d) Dissociation curves at increasing values of λ_x ($\omega = 2$ eV).

we study in this work is the interaction of a single photon with the two electrons of an H_2 molecule in an optical cavity, as illustrated in Figure 1(a). In section 3A of the Supporting Information, we show the advantage of the QED-UCCSD-1 method by tabulating energies calculated using the QED-HF and QED-UCCSD-1 methods for this system. We use the full configuration interaction (FCI) energy as a reference against which we assess accuracy. In addition, we compare the FCI average photon numbers with those calculated using the QED-UCCSD-1 method. This is done with respect to both bond length and coupling strength.

An implementation of the VQE-PUCC method on a quantum device follows the standard procedure.[39,49] In the first step, the second-quantized Hamiltonian from eq 1 is constructed by using the QED-HF spin−orbitals. In the second step, the fermionic and bosonic operators that occur in both the Hamiltonian and cluster operators are converted into the I, X, Y, and Z Pauli basis. Due to different spin statistics between electrons (fermions) and photons (bosons), their corresponding creation/annihilation operators are mapped to the qubit basis differently. The fermionic creation and annihilation operators are converted into the qubit basis with Jordan−Wigner mapping[50] or with a more economic Bravyi−Kitaev mapping.[51,52] The latter approach allows the removal of two qubits, thereby significantly reducing the quantum hardware requirements.[53] The bosonic creation and annihilation operators can be converted to the qubit basis by the direct boson mapping[54−56] in which the state with n bosons is mapped to $n + 1$ qubits. With the direct boson mapping, the bosonic creation operator is transformed as

$$b^\dagger = \sum_{j=0}^{n-1} \sqrt{j+1}\,\sigma_+^j \sigma_-^{j+1} \tag{7}$$

where $\sigma_\pm = 1/2(X \pm iY)$. Moreover, we will also calculate the photon number operator that is transformed as

$$b^\dagger b = \sum_{j=0}^{n} j \frac{Z^j + I}{2} \tag{8}$$

Following the conversion of second-quantized operators to the qubit basis, state preparation with the PUCC ansatz, and energy measurement on a noisy quantum computer, the optimization of the wave function parameters $\theta_{\mu,n}$ is performed on a classical computer. This step is repeated until convergence in energy is achieved.

For electron−photon systems, we can exploit an additional symmetry to reduce the number of necessary qubits in the simulation. After applying the Bravyi−Kitaev mapping that results in two fewer qubits compared to the Jordan−Wigner mapping, we can taper off an additional qubit by exploiting the total parity operator, which is a $\mathcal{Z}_2$ symmetry.[53,57] For the electron−photon system studied here, the total parity operator $\mathcal{P} = \mathcal{P}_e \cdot \mathcal{P}_{ph}$ is the product of the electronic parity $\mathcal{P}_e$ and the photon parity operator $\mathcal{P}_{ph}$ that is defined as

$$\mathcal{P}_{ph} = \exp(-i\pi b^\dagger b) \tag{9}$$

Therefore, using the Bravyi−Kitaev mapping, direct boson mapping, and the parity symmetry, we can describe the system by $n - 3$ qubits compared to n qubits needed in the Jordan−Wigner and direct boson mapping alone. Figure 1(b) shows the ansatz after undergoing Bravyi−Kitaev mapping and qubit tapering. Table 1 shows the number of qubits and CNOT gates associated with different mappings.

Table 1. Dimensions of the Cluster Excitation Operator for H_2 in a Cavity for Different Fermion-to-Qubit Mappings[a]

Mapping	Qubits	CNOTs
Jordan−Wigner (JW)	5	96
Bravyi−Kitaev (BK)	3	10
BK + Tapering	2	2

[a]By leveraging $\mathcal{Z}_2$ symmetries, we reduce the circuit to two qubits and two entangling CNOT gates.

Experimentally relevant electron−photon coupling strengths result in comparatively small differences in observables. For instance, ground-state energy shifts between experimentally realizable ranges of λ are expected to be on the order of meV.[27] As an example, Figure 1(c) shows FCI calculations for the energy difference between the ground-state energy of an H_2 molecule outside the optical cavity (i.e., $\lambda = 0$ a.u.) and the ground-state energy for finite values of λ_x (where $\omega = 2$ eV).

https://doi.org/10.1021/acs.jpclett.3c02875
J. Phys. Chem. Lett. 2024, 15, 1373−1381

These results give an estimate of how high the resolution of the noisy VQE approach must be to resolve energy differences between λ_x. For example, the energy difference between $\lambda_x = 0$ a.u. and $\lambda_x = 0.1$ a.u. in Figure 1(c) is 7.8 mHa. Similarly, the FCI calculations in Figure 1(d) show how the bond-length-dependent energy, or dissociation curve, also shifts on the order of mHa across the relevant range of λ_x. We find the equilibrium bond length shifting from 0.735 Å for $\lambda_x = 0$ a.u. to 0.726 Å for $\lambda_x = 0.2$ a.u. Additionally, we find for the energy difference between $\lambda_x = 0$ a.u. and $\lambda_x = 0.05$ a.u. a value of 1.96 mHa, which is close to the standard of chemical accuracy of 1.6 mHa (~43 meV) in electronic-structure calculations. Thus, these small energy differences in the weak coupling regime, and in particular if $\lambda < 0.05$ a.u., set an additional criterion for the precision of the quantum simulation. Not only must the results be within the criteria for chemical accuracy, but the noise level must fall within the energy difference to correctly resolve it. In section 1 of the Supporting Information, we show the energy dependence on cavity frequency by plotting the change in energy (with respect to cavity frequency) relative to the energy of bare H_2 at equilibrium bond length (i.e., $\lambda_x = 0$ a.u.).

To resolve these differences in small, noisy quantum devices in practice, we employ error mitigation. In this work, we compose several methods: readout-error mitigation,[58] zero-noise extrapolation (ZNE),[59−61] and reference-state zero-noise extrapolation (rZNE),[62] which is a combination of reference-state (RS) error mitigation[62] and ZNE.[59−61]

The key idea behind ZNE is that the application of a unitary gate, succeeded by the application of its inverse, produces an identity for a noiseless device. Thus, if the whole circuit U is unitary, its copy U and its inverse U^{-1} can be appended to the end of the circuit, i.e., $U = UU^{-1}U$. On a noisy device, this procedure has the effect of amplifying the noise of the original circuit. The degree of noise amplification is defined by the noise factor m, where $m = 2n + 1$ and n is the number of times that a copy of the circuit and its inverse is applied, i.e., $U = U(U^{-1}U)^n$. The expectation value of the unitary is measured at different noise factors, and then, these noisy expectation values are used to extrapolate the gate-error-free expectation value at a noise factor of 0.

To further reduce errors, we rely on the RS error mitigation. Here, the noise of the quantum device is treated as an operation which rescales the exact expectation value into the measured expectation value, i.e.,

$$\langle \vec{\theta}|\hat{O}|\vec{\theta}\rangle_{\text{noisy}} = r\langle \vec{\theta}|\hat{O}|\vec{\theta}\rangle_{\text{exact}} \tag{10}$$

where $\hat{O}$ is an arbitrary operator, $\vec{\theta}$ are the parameters of the ansatz, and r is the rescale factor. To obtain these rescaling factors, this approach makes use of reference states: states for which the exact expectation values are known or can be constructed noise-free. For the electron−photon systems discussed here, we can use the QED-HF state, where all parameters in the PUCC ansatz are set to 0, as a reference state. The rescale factor is then the ratio of the measured QED-HF energy on the quantum device to the numerically exact QED-HF state obtained from standard electronic-structure packages. The rescale factors can then be used in eq 10 to obtain the unbiased expectation value in any arbitrary state. The underlying assumption here is that the noise of the quantum device is only weakly dependent on the specific ansatz parameters. RS mitigation can be combined with other error mitigation techniques as long as the same combination of mitigation techniques is used for measuring in both the reference state and the desired state.

The rZNE mitigation strategy works by using the ZNE fitting functions of both the reference state and the desired state to calibrate the noisy expectation value. This method is based on the assumption that the noise between two qubits can be modeled as a depolarizing channel, an assumption which holds well for IBM's devices under Pauli twirling.[63] The depolarizing channel can be mathematically expressed as such: $\rho_2 \rightarrow (1 - p_m)\rho_2 + p_m \frac{I \otimes I}{4}$, where ρ_2 is the density matrix representing the state of the two qubits, p_m is the depolarizing probability given by $p_m = 1 - e^{-gm}$, m is the noise factor, and g is the device and gate-dependent exponential decay constant that governs how drastically the noise is amplified at a given noise factor. This function is chosen such that if the noise factor becomes large, the density matrix becomes maximally mixed, while when the noise factor goes to zero, the density matrix remains unchanged. It follows that when applying ZNE, the fitting function has the following exponential form: $f(m) = Ee^{-gm}$, where E is the energy being measured. To combine the RS mitigation with ZNE, we apply ZNE both when measuring the reference state and when running the VQE algorithm. We obtain the ZNE fitting function for both as such: $f_r(m) = a_r e^{-g_r m} + c_r$ for the reference state and $f_e(m) = a_e e^{-g_e m} + c_e$ for the VQE result, where the subscripts r and e denote fitting parameters for the reference state and VQE result, respectively. We note that at zero-noise ($m = 0$), $f_r(0) = E_{\text{QED-HF}} = a_r + c_r$ and $f_e(0) = E_{\text{unbiased}} = a_e + c_e$, where $E_{\text{QED-HF}}$ is the QED-HF energy and E_{unbiased} is the energy obtained from the VQE with zero gate noise. We note that in practice, when ZNE is applied, the fitting functions contain the additive parameters c_r and c_e for the reference and VQE energies, respectively. Since the energies at $m = 0$ still contain noise, we can rescale as such: $E_{\text{QED-HF}} = a_r \cdot r + c_r$ and $E_{\text{unbiased}} = a_e \cdot r + c_e$, where r is the rescale factor. We combine the expressions for the rescale factors with the fitting functions to obtain the following energy expression:

$$E_{\text{rZNE}} = a_e \frac{E_{\text{QED-HF}} - c_r}{a_r} + c_e \tag{11}$$

In eq 11, E_{rZNE} is the rZNE mitigated VQE energy. We combine rZNE with readout error mitigation by mitigating the readout error for the energy at each noise factor for both the reference state and VQE measurements. In section 3B of the Supporting Information, we tabulate the rZNE fit parameters with respect to bond length and coupling strength.

To further reduce the error, we found that it is possible to map the occupied states to $|0\rangle$, which is less susceptible to processes leading to in particular amplitude damping.[64] For the H_2 molecule, there are two electrons; therefore, two of the spin−orbitals must be occupied. In the ansatz circuit, this is done by initializing the qubits in the $|1\rangle$ state by operating on each qubit with an X-gate, as shown in Figure 1(b). In the context of superconducting qubits, a qubit is a two level system in which the $|0\rangle$ state is the ground state and the $|1\rangle$ state is the excited state. Since the $|1\rangle$ state is an excited state, energy loss in the qubit causes the $|1\rangle$ state to irreversibly decay into the $|0\rangle$ state after a finite time, so it is generally more ideal to start off in the $|0\rangle$ state if possible. We avoid initializing the qubits in the $|1\rangle$ state by multiplying the coefficients of each term in the mapped Hamiltonian by $(-1)^k$, where k is the number of Z-gates that appear in that term. Table 2 compares the results between an ansatz with X-gates and the ansatz without X-gates.

https://doi.org/10.1021/acs.jpclett.3c02875
J. Phys. Chem. Lett. 2024, 15, 1373−1381

Table 2. VQE Results for Polaritonic H_2 with ω = 2 eV and λ_x = 0.1 a.u. at Equilibrium Bond Length[a]

Ansatz Initialization	E [Ha]	% Error	Std [Ha]
$\|1\rangle$ (With X gates)	−1.0925	3.2709	0.0019
$\|0\rangle$ (No X gates)	−1.1035	2.2997	0.0016

[a]We compare the results for when the ansatz is initialized in the $|1\rangle$ state (by applying X-gates to the beginning of the ansatz) and the $|0\rangle$ state. For each case, the result is the average of 20 VQE runs. The FCI energy in this case is −1.1295 Ha. The last column shows the standard deviation.

From this, we find that the ansatz with X-gates gives a result with a percent error of 3.2709%, while the ansatz without X-gates gives a result with a percent error of 2.2997%. This result shows that removing the X-gates indeed gives a small advantage in accuracy while also reducing computational resources.

In this work, we run all simulations using the Qiskit platform.[65] Qiskit offers tools called "Fake Devices" which allow us to simulate real IBM devices. This is done by extracting characteristics of the device's qubits and quantum gates and using them as parameters to generate a noise model. The noise model assumes that the noise of the quantum computer can be modeled using a depolarizing channel and an amplitude-phase damping channel with the addition of readout error after measurement. To this end, IBM records the relaxation time (T_1), the dephasing time (T_2), the readout error, gate errors, and gate lengths of the device. The readout error is used to determine the probability of measuring a 0 after preparing a 1 and vice versa. T_1 is a time constant that dictates how long it takes the $|1\rangle$ state to lose energy and decay into the $|0\rangle$ state. T_2 is also a time constant that dictates the loss of relative phase in the qubit state. T_1 and T_2 are used in calculating the probabilities for the amplitude and phase damping. The gate errors are used for calculating the probability for the depolarizing channel. The noise model allows us to generate noise in our simulations which mimic the noise of the actual device. In this work, we use the calibration data of the IBM Cairo device for our noisy quantum simulations. IBM Cairo was chosen because it has longer T_1 and T_2 time constants as well as lower CNOT and readout assignment errors relative to IBM's other devices. In section 4 of the Supporting Information, we tabulate the T_1 and T_2 time constants, the readout error, gate errors, and gate lengths of the device, along with the dates on which those parameters were reported.

All of the simulations are run with twenty thousand shots. For each data point, ten VQE simulations are run, and the average result of these ten runs is plotted. The error bars shown are the root-mean-square error (RMSE) of these ten runs.

Readout-error mitigation is applied using the M3 package.[58] We use M3 by sampling the calibration data from two physical qubits on the fake device (which can also be done on the real device) and then mapping the virtual qubits of our system to those same physical qubits. The measurement of the system is then corrected by the calibration data during every function evaluation of the VQE loop.

In implementing ZNE, we only scale the CNOT gates. We use scale factors of 1, 3, 5, 51, 101, and 201. Using these scale factors allows us to properly fit the measured expectation values to an exponential so that we can obtain the fitting parameters for use in eq 11. ZNE is applied during each objective function evaluation. Unlike readout-error mitigation and ZNE, RS mitigation and rZNE are only applied to the final converged VQE results. When calculating the rescale factors for reference-state mitigation and the reference exponential fit parameters for rZNE, we measure the noisy QED-HF state 50 times and take the average.

We now discuss the results obtained by using the IBM Cairo simulator. Figure 2(a) shows the dissociation curve of the H_2 molecule inside an optical cavity. In the plot, we show the ground-state energy changing with different bond lengths, where the bond length is defined by the distance between the two hydrogen atoms. In this case, the cavity frequency is chosen as ω = 2 eV and the coupling strength is chosen as λ_x = 0.1 a.u., with the coupling strength in the other directions set to zero. These parameter values are chosen in agreement with previous work.[25,66] The VQE results are plotted for different levels of error mitigation.

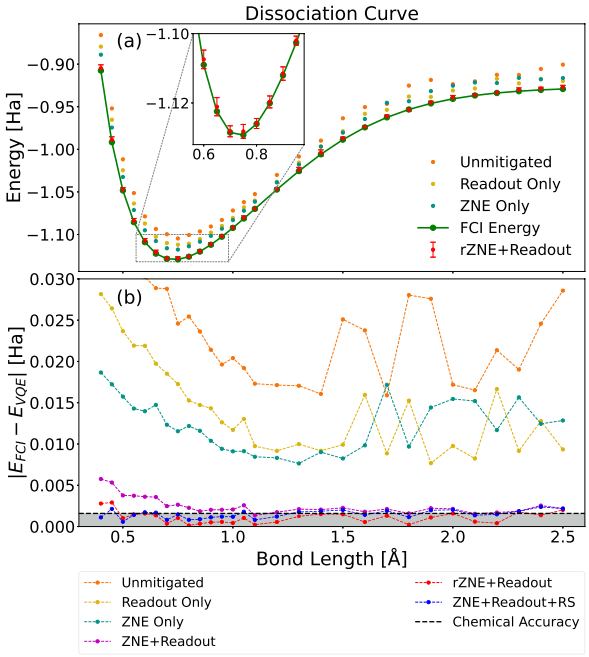

Figure 2. (a) Potential energy surface for H_2 coupled to a single photon mode. Results are shown for different levels of error mitigation. The inset shows the error bars near equilibrium. (b) The error relative to the FCI energies for different levels of error mitigation. The gray shaded region is the region in which the results are chemically accurate. The first few points for the unmitigated energies are cutoffs due to high errors. The results obtained using combinations of ZNE, readout-error mitigation, and RS mitigation are not shown in (a) due to their close overlap with the rZNE results, but their associated errors are shown in (b). Chemical accuracy can be achieved with combinations of ZNE, readout-error mitigation, and RS mitigation and can consistently be achieved with rZNE.

Figure 2(b) shows the relative error as the absolute value of the difference between the FCI energy and the VQE energy in Figure 2(a). We find that we are able to achieve chemical accuracy for many of the bond lengths when combining rZNE with readout-error mitigation and when combining ZNE with readout-error mitigation and RS mitigation. However, for the combination of readout-error mitigation with ZNE, most of the results are just outside of chemical accuracy. This shows quantum computing is a promising avenue for studying

https://doi.org/10.1021/acs.jpclett.3c02875
J. Phys. Chem. Lett. 2024, 15, 1373−1381

electron−photon problems, even in the near term, due to the unique advantage that electron−photon reference states have for enhancing error mitigation.

In the following, we further explore the robustness of the VQE-PUCC approach across various coupling strengths. To quantify the performance, we measure two properties: the ground-state energy, which is fundamentally relevant to chemical reactivity, and the photon number, which is a general indicator of how correlated the electron−photon system is and can be monitored experimentally.

Thus, Figure 3(a) shows the VQE results for the energy at different coupling strengths for photon polarization along the

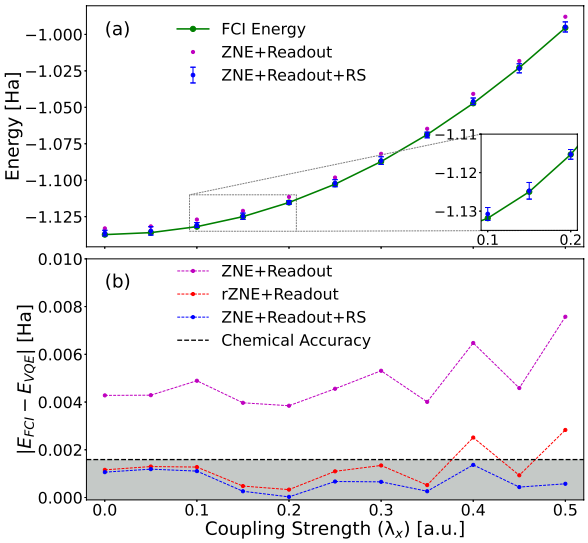

Figure 3. (a) Energy with respect to coupling strength in the x-direction for H_2 coupled to a single photon in single photon mode. Results are shown for different levels of error mitigation. (b) The error relative to the FCI energies for different levels of error mitigation. The shaded region is the region in which the results are chemically accurate.

x-direction. The cavity frequency is set to ω = 20 eV. The bond length at each data point is the equilibrium bond length for the given ω and associated λ_x. The purpose of the inset is to show the scale of the error bars.

Figure 3(b) shows the relative error as the absolute value of the difference between the FCI energy and the VQE energies in Figure 3(a). Unlike Figure 2, where rZNE generally performs better than RS mitigation, in this case, RS mitigation performs better than rZNE. In fact, RS mitigation gives chemically accurate results for points.

Figure 4 shows the average photon number. The average photon number is calculated as $\langle b^\dagger b\rangle = \frac{1}{2}(1 - \langle ZZ\rangle)$, where $\langle b^\dagger b\rangle$ is the average photon number and ZZ is the operator that represents the application of a Pauli-Z gate on each of the two qubits. The expectation value is computed using the ground state of the Hamiltonian. To obtain the average photon number in the ground state on a quantum computer as shown in Figure 4(a), we use the ZZ expectation value at the optimal points found by the VQE. These are the same optimal points that give the energies in Figure 3(a). The reference exponential fit parameters for rZNE are found by measuring $\langle b^\dagger b\rangle$ in the QED-HF state at different scale factors. For RS mitigation, since the exact result for $\langle b^\dagger b\rangle$ in the QED-HF state is zero,

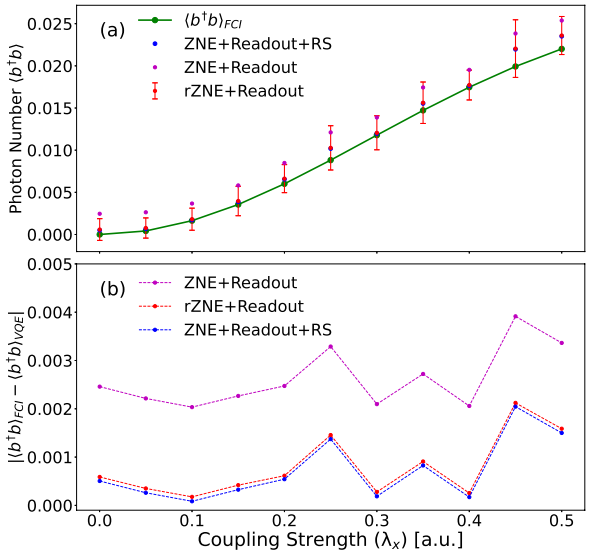

Figure 4. (a) Average photon number with respect to coupling strength in the x-direction for H_2 coupled to a single photon in single photon mode. Results are shown for different levels of error mitigation. (b) The error relative to the FCI average photon number for different levels of error mitigation.

calculating the rescale factor would result in a division by zero. What we do instead is measure $\langle ZZ\rangle$ in the QED-HF state. Since the exact expectation value of the ZZ operator is one, the rescale factor is the noisy measurement of $\langle ZZ\rangle$ in the QED-HF state. We use this rescale factor to rescale the noisy measurement of $\langle ZZ\rangle$ in the optimal state. We find that even though the optimal points found by the VQE allow for convergence of the energy with small error bars, this does not necessarily mean that the photon number at those optimal points will have similarly small error bars. In section 2 of the Supporting Information, we replot Figure 3 and Figure 4 for a cavity frequency of 2 eV. We find that the error bars for the photon numbers are large compared to those of Figure 4. Additionally, even though the absolute errors of the photon numbers at 2 and 20 eV are similar, the small value of the photon number at 2 eV makes the relative error larger than the relative errors at 20 eV. Thus, simulations for small photon numbers are more susceptible to noise. Simulating the system at a cavity frequency of 20 eV allows us to simulate photon numbers that are much higher than the noise level. Though such a high cavity frequency might be hard to realize in a lab, it allows us to demonstrate the ability of the VQE to simulate observables other than energy. We observe that even though the combination of readout-error mitigation and RS mitigation is more accurate than readout-error mitigation and rZNE when calculating the energy (Figure 3), rZNE is more accurate than RS mitigation when calculating the average photon number.

The convergence data for the VQE simulations are listed in Figure 5. Figure 5(a) shows the average number of iterations for the results shown in Figure 3(a). For each λ_x, we average the number of iterations for the 10 VQE results and plot the average in Figure 5(a). Similarly, in Figure 5(b), we plot the average number of iterations over the ten VQE results from 2(a) for each bond length and each error mitigation technique. We find that as the coupling strength increases, the number of iterations required to converge decreases. We also find that using readout-error mitigation and ZNE together greatly

https://doi.org/10.1021/acs.jpclett.3c02875
J. Phys. Chem. Lett. 2024, 15, 1373−1381

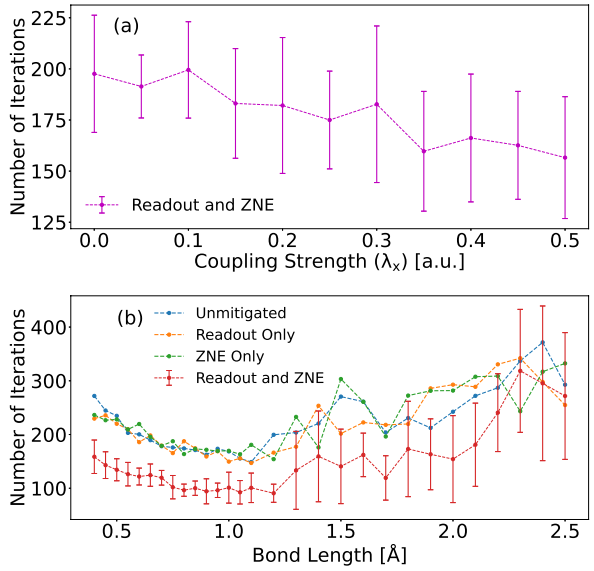

Figure 5. (a) The average number (n = 10) of iterations that it takes for the VQE to converge vs the coupling strength in the x-direction (λ_x). (b) The average number (n = 10) of iterations that it takes for the VQE to converge vs the bond length. In both subplots, the error bars are the standard deviation of the iterations.

reduces the required number of iterations, but this does not reduce the simulation time due to the overhead necessary to execute these mitigation techniques.

In this work, we show the viability of the PUCC ansatz for calculating the ground-state energy by using the VQE algorithm on realistic noise models. Furthermore, we use the optimized parameters from VQE to calculate the average photon number. The performance of this method is tested on an H_2 molecule interacting with a single photon in a single cavity mode. We use Qiskit's noisy simulators to obtain ground-state energies across different regimes of bond lengths, cavity frequencies, and coupling strengths. Additionally, we employ various error mitigation techniques and show that the availability of reference states for electron−photon problems offers unique advantages in achieving chemically accurate results. Our VQE results for the ground-state energies are in excellent agreement with the FCI results, with many of the VQE results falling within chemical accuracy. Future work will include the calculation of excited-state energies[25,67,68] using the quantum electrodynamic equation-of-motion (QED-qEOM) method which was developed alongside the PUCC ansatz.[25] The methods presented in this work open up many additional research directions for developments in computational polaritonic quantum chemistry using quantum computing as well as using quantum devices for strongly coupled fermion−boson systems.

■ ASSOCIATED CONTENT

Supporting Information

The Supporting Information is available free of charge at https://pubs.acs.org/doi/10.1021/acs.jpclett.3c02875.

Energy dependence on cavity frequency and plot of FCI calculations, VQE energy and photon number with respect to coupling strength at a cavity frequency of 2 eV on a noisy simulator, numerical data used in the manuscript (FCI, QED-HF, and PUCC energies and rZNE fit parameters), and IBM Cairo noise parameters (PDF)

Transparent Peer Review report available (PDF)

■ AUTHOR INFORMATION

Corresponding Authors

Fabijan Pavošević − *Algorithmiq Ltd., FI-00160 Helsinki, Finland;* orcid.org/0000-0002-3693-7546; Email: fpavosevic@gmail.com

Johannes Flick − *Department of Physics, City College of New York, New York, New York 10031, United States; Department of Physics, The Graduate Center, City University of New York, New York, New York 10016, United States; Center for Computational Quantum Physics, Flatiron Institute, New York, New York 10010, United States;* orcid.org/0000-0003-0273-7797; Email: jflick@ccny.cuny.edu

Authors

Mohammad Hassan − *Department of Physics, City College of New York, New York, New York 10031, United States; Department of Physics, The Graduate Center, City University of New York, New York, New York 10016, United States*

Derek S. Wang − *Harvard John A. Paulson School of Engineering and Applied Sciences, Harvard University, Cambridge, Massachusetts 02138, United States;* orcid.org/0000-0003-4538-5816

Complete contact information is available at: https://pubs.acs.org/10.1021/acs.jpclett.3c02875

Notes

The authors declare no competing financial interest.

■ ACKNOWLEDGMENTS

We acknowledge startup funding from the City College of New York. J.F. and M.H. acknowledges funding from the NSF through grant NSF-2216838 and the NSF Phase II CREST Center IDEALS with grant no. EES-2112550. The Flatiron Institute is a division of the Simons Foundation.

■ REFERENCES

(1) Ebbesen, T. W. Hybrid Light−Matter States in a Molecular and Material Science Perspective. *Acc. Chem. Res.* **2016**, *49*, 2403−2412.

(2) Ruggenthaler, M.; Tancogne-Dejean, N.; Flick, J.; Appel, H.; Rubio, A. From a Quantum-Electrodynamical Light-Matter Description to Novel Spectroscopies. *Nat. Rev. Chem.* **2018**, *2*, 0118.

(3) Flick, J.; Rivera, N.; Narang, P. Strong light-matter coupling in quantum chemistry and quantum photonics. *Nanophotonics* **2018**, *7*, 1479−1501.

(4) Garcia-Vidal, F. J.; Ciuti, C.; Ebbesen, T. W. Manipulating matter by strong coupling to vacuum fields. *Science* **2021**, *373*, eabd0336.

(5) Fregoni, J.; Garcia-Vidal, F. J.; Feist, J. Theoretical Challenges in Polaritonic Chemistry. *ACS Photonics* **2022**, *9*, 1096−1107.

(6) Yuen-Zhou, J.; Xiong, W.; Shegai, T. Polariton chemistry: Molecules in cavities and plasmonic media. *J. Chem. Phys.* **2022**, *156*, No. 030401.

(7) Mandal, A.; Taylor, M. A.; Weight, B. M.; Koessler, E. R.; Li, X.; Huo, P. Theoretical Advances in Polariton Chemistry and Molecular Cavity Quantum Electrodynamics. *Chem. Rev.* **2023**, *123*, 9786−9879.

(8) Frisk Kockum, A.; Miranowicz, A.; De Liberato, S.; Savasta, S.; Nori, F. Ultrastrong coupling between light and matter. *Nat. Rev. Phys.* **2019**, *1*, 19−40.

(9) Benz, F.; Schmidt, M. K.; Dreismann, A.; Chikkaraddy, R.; Zhang, Y.; Demetriadou, A.; Carnegie, C.; Ohadi, H.; De Nijs, B.; Esteban, R.; et al. Single-molecule optomechanics in "picocavities. *Science* **2016**, *354*, 726−729.
(10) Baumberg, J. J. Picocavities: A Primer. *Nano Lett.* **2022**, *22*, 5859−5865.
(11) Thomas, A.; George, J.; Shalabney, A.; Dryzhakov, M.; Varma, S. J.; Moran, J.; Chervy, T.; Zhong, X.; Devaux, E.; Genet, C.; et al. Ground-State Chemical Reactivity under Vibrational Coupling to the Vacuum Electromagnetic Field. *Angew. Chem., Int. Ed.* **2016**, *128*, 11634−11638.
(12) Thomas, A.; Lethuillier-Karl, L.; Nagarajan, K.; Vergauwe, R. M.; George, J.; Chervy, T.; Shalabney, A.; Devaux, E.; Genet, C.; Moran, J.; et al. Tilting a Ground-state Reactivity Landscape by Vibrational Strong Coupling. *Science* **2019**, *363*, 615−619.
(13) Ahn, W.; Triana, J. F.; Recabal, F.; Herrera, F.; Simpkins, B. S. Modification of ground-state chemical reactivity via light−matter coherence in infrared cavities. *Science* **2023**, *380*, 1165−1168.
(14) Fregoni, J.; Granucci, G.; Coccia, E.; Persico, M.; Corni, S. Manipulating Azobenzene Photoisomerization through Strong Light−molecule Coupling. *Nat. Commun.* **2018**, *9*, 4688.
(15) Climent, C.; Galego, J.; Garcia-Vidal, F. J.; Feist, J. Plasmonic Nanocavities Enable Self-Induced Electrostatic Catalysis. *Angew. Chem., Int. Ed.* **2019**, *58*, 8698−8702.
(16) Li, X.; Mandal, A.; Huo, P. Cavity Frequency-dependent Theory for Vibrational Polariton Chemistry. *Nat. Commun.* **2021**, *12*, 1315.
(17) Campos-Gonzalez-Angulo, J. A.; Yuen-Zhou, J. Polaritonic normal modes in transition state theory. *J. Chem. Phys.* **2020**, *152*, 161101.
(18) Sánchez-Barquilla, M.; Fernández-Domínguez, A. I.; Feist, J.; García-Vidal, F. J. A theoretical perspective on molecular polaritonics. *ACS Photonics* **2022**, *9*, 1830−1841.
(19) Tokatly, I. V. Time-Dependent Density Functional Theory for Many-Electron Systems Interacting with Cavity Photons. *Phys. Rev. Lett.* **2013**, *110*, 233001.
(20) Ruggenthaler, M.; Flick, J.; Pellegrini, C.; Appel, H.; Tokatly, I. V.; Rubio, A. Quantum-Electrodynamical Density-Functional Theory: Bridging Quantum Optics and Electronic-Structure Theory. *Phys. Rev. A* **2014**, *90*, No. 012508.
(21) Flick, J. Simple exchange-correlation energy functionals for strongly coupled light-matter systems based on the fluctuation-dissipation theorem. *Phys. Rev. Lett.* **2022**, *129*, 143201.
(22) Vu, N.; McLeod, G. M.; Hanson, K.; DePrince, A. E., III Enhanced Diastereocontrol via Strong Light−Matter Interactions in an Optical Cavity. *J. Phys. Chem. A* **2022**, *126*, 9303−9312.
(23) Haugland, T. S.; Ronca, E.; Kjønstad, E. F.; Rubio, A.; Koch, H. Coupled Cluster Theory for Molecular Polaritons: Changing Ground and Excited States. *Phys. Rev. X* **2020**, *10*, No. 041043.
(24) DePrince, A. E., III Cavity-Modulated Ionization Potentials and Electron Affinities from Quantum Electrodynamics Coupled-Cluster Theory. *J. Chem. Phys.* **2021**, *154*, No. 094112.
(25) Pavošević, F.; Flick, J. Polaritonic Unitary Coupled Cluster for Quantum Computations. *J. Phys. Chem. Lett.* **2021**, *12*, 9100−9107.
(26) Pavošević, F.; Rubio, A. Wavefunction Embedding for Molecular Polaritons. *J. Chem. Phys.* **2022**, *157*, No. 094101.
(27) Pavošević, F.; Hammes-Schiffer, S.; Rubio, A.; Flick, J. Cavity-Modulated Proton Transfer Reactions. *J. Am. Chem. Soc.* **2022**, *144*, 4995−5002.
(28) Schäfer, C.; Flick, J.; Ronca, E.; Narang, P.; Rubio, A. Shining Light on the Microscopic Resonant Mechanism Responsible for Cavity-Mediated Chemical Reactivity. *Nat. Commun.* **2022**, *13*, 7817.
(29) Pavošević, F.; Smith, R. L.; Rubio, A. Computational Study on the Catalytic Control of endo/exo Diels-Alder Reactions by Cavity Quantum Vacuum Fluctuations. *Nat. Commun.* **2023**, *14*, 2766.
(30) Pavošević, F.; Smith, R. L.; Rubio, A. Cavity Click Chemistry: Cavity-Catalyzed Azide−Alkyne Cycloaddition. *J. Phys. Chem. A* **2023**, *127*, 10184−10188.
(31) Lyakh, D. I.; Musiał, M.; Lotrich, V. F.; Bartlett, R. J. Multireference Nature of Chemistry: The Coupled-Cluster View. *Chem. Rev.* **2012**, *112*, 182−243.
(32) Szalay, P. G.; Müller, T.; Gidofalvi, G.; Lischka, H.; Shepard, R. Multiconfiguration Self-Consistent Field and Multireference Configuration Interaction Methods and Applications. *Chem. Rev.* **2012**, *112*, 108−181.
(33) Cao, Y.; Romero, J.; Olson, J. P.; Degroote, M.; Johnson, P. D.; Kieferová, M.; Kivlichan, I. D.; Menke, T.; Peropadre, B.; Sawaya, N. P.; et al. Quantum Chemistry in the Age of Quantum Computing. *Chem. Rev.* **2019**, *119*, 10856−10915.
(34) Bauer, B.; Bravyi, S.; Motta, M.; Kin-Lic Chan, G. Quantum Algorithms for Quantum Chemistry and Quantum Materials Science. *Chem. Rev.* **2020**, *120*, 12685−12717.
(35) Head-Marsden, K.; Flick, J.; Ciccarino, C. J.; Narang, P. Quantum Information and Algorithms for Correlated Quantum Matter. *Chem. Rev.* **2021**, *121*, 3061−3120.
(36) Aspuru-Guzik, A.; Dutoi, A. D.; Love, P. J.; Head-Gordon, M. Simulated Quantum Computation of Molecular Energies. *Science* **2005**, *309*, 1704−1707.
(37) Lanyon, B. P.; Whitfield, J. D.; Gillett, G. G.; Goggin, M. E.; Almeida, M. P.; Kassal, I.; Biamonte, J. D.; Mohseni, M.; Powell, B. J.; Barbieri, M.; et al. Towards Quantum Chemistry on a Quantum Computer. *Nat. Chem.* **2010**, *2*, 106−111.
(38) Preskill, J. Quantum Computing in the NISQ era and beyond. *Quantum* **2018**, *2*, 79.
(39) Peruzzo, A.; McClean, J.; Shadbolt, P.; Yung, M.-H.; Zhou, X.-Q.; Love, P. J.; Aspuru-Guzik, A.; O'brien, J. L. A Variational Eigenvalue Solver on a Photonic Quantum Processor. *Nat. Commun.* **2014**, *5*, 4213.
(40) Shen, Y.; Zhang, X.; Zhang, S.; Zhang, J.-N.; Yung, M.-H.; Kim, K. Quantum Implementation of the Unitary Coupled Cluster for Simulating Molecular Electronic Structure. *Phys. Rev. A* **2017**, *95*, No. 020501.
(41) Hempel, C.; Maier, C.; Romero, J.; McClean, J.; Monz, T.; Shen, H.; Jurcevic, P.; Lanyon, B. P.; Love, P.; Babbush, R.; et al. Quantum Chemistry Calculations on a Trapped-Ion Quantum Simulator. *Phys. Rev. X* **2018**, *8*, No. 031022.
(42) O'Malley, P. J.; Babbush, R.; Kivlichan, I. D.; Romero, J.; McClean, J. R.; Barends, R.; Kelly, J.; Roushan, P.; Tranter, A.; Ding, N.; et al. Scalable Quantum Simulation of Molecular Energies. *Phys. Rev. X* **2016**, *6*, No. 031007.
(43) Kandala, A.; Mezzacapo, A.; Temme, K.; Takita, M.; Brink, M.; Chow, J. M.; Gambetta, J. M. Hardware-efficient Variational Quantum Eigensolver for Small Molecules and Quantum Magnets. *Nature* **2017**, *549*, 242−246.
(44) Rossmannek, M.; Pavošević, F.; Rubio, A.; Tavernelli, I. Quantum Embedding Method for the Simulation of Strongly Correlated Systems on Quantum Computers. *J. Phys. Chem. Lett.* **2023**, *14*, 3491−3497.
(45) Pavošević, F.; Culpitt, T.; Hammes-Schiffer, S. Multi-component Coupled Cluster Singles and Doubles Theory within the Nuclear-Electronic Orbital Framework. *J. Chem. Theory Comput.* **2019**, *15*, 338−347.
(46) Pavošević, F.; Culpitt, T.; Hammes-Schiffer, S. Multi-component Quantum Chemistry: Integrating Electronic and Nuclear Quantum Effects via the Nuclear-Electronic Orbital Method. *Chem. Rev.* **2020**, *120*, 4222−4253.
(47) Pavošević, F.; Hammes-Schiffer, S. Multicomponent Unitary Coupled Cluster and Equation-of-Motion for Quantum Computation. *J. Chem. Theory Comput.* **2021**, *17*, 3252−3258.
(48) Romero, J.; Babbush, R.; McClean, J. R.; Hempel, C.; Love, P. J.; Aspuru-Guzik, A. Strategies for Quantum Computing Molecular Energies Using the Unitary Coupled Cluster Ansatz. *Quant. Sci. Techn.* **2019**, *4*, No. 014008.
(49) Tilly, J.; Chen, H.; Cao, S.; Picozzi, D.; Setia, K.; Li, Y.; Grant, E.; Wossnig, L.; Rungger, I.; Booth, G. H.; et al. The Variational Quantum Eigensolver: A Review of Methods and Best Practices. *Phys. Rep.* **2022**, *986*, 1−128.

https://doi.org/10.1021/acs.jpclett.3c02875
J. Phys. Chem. Lett. 2024, 15, 1373−1381

(50) Jordan, P.; Neumann, J. v.; Wigner, E. P. *The Collected Works of Eugene Paul Wigner*; Springer, 1993; pp 298−333.
(51) Bravyi, S. B.; Kitaev, A. Y. Fermionic Quantum Computation. *Ann. Phys.* **2002**, *298*, 210−226.
(52) Seeley, J. T.; Richard, M. J.; Love, P. J. The Bravyi-Kitaev Transformation for Quantum Computation of Electronic Structure. *J. Chem. Phys.* **2012**, *137*, 224109.
(53) Bravyi, S.; Gambetta, J. M.; Mezzacapo, A.; Temme, K. Tapering off qubits to simulate fermionic Hamiltonians. *arXiv:1701.08213* **2017**, DOI: 10.48550/arXiv.1701.08213.
(54) Somma, R.; Ortiz, G.; Knill, E.; Gubernatis, J. Quantum Simulations of Physics Problems. *Int. J. Quantum Chem.* **2003**, *1*, 189−206.
(55) Veis, L.; Višňák, J.; Nishizawa, H.; Nakai, H.; Pittner, J. Quantum chemistry beyond Born−Oppenheimer approximation on a quantum computer: A simulated phase estimation study. *Int. J. Quantum Chem.* **2016**, *116*, 1328−1336.
(56) Macridin, A.; Spentzouris, P.; Amundson, J.; Harnik, R. Electron-Phonon Systems on a Universal Quantum Computer. *Phys. Rev. Lett.* **2018**, *121*, 110504.
(57) Setia, K.; Chen, R.; Rice, J. E.; Mezzacapo, A.; Pistoia, M.; Whitfield, J. D. Reducing Qubit Requirements for Quantum Simulations Using Molecular Point Group Symmetries. *J. Chem. Theory Comput.* **2020**, *16*, 6091−6097.
(58) Nation, P. D.; Kang, H.; Sundaresan, N.; Gambetta, J. M. Scalable Mitigation of Measurement Errors on Quantum Computers. *PRX Quantum* **2021**, *2*, No. 040326.
(59) Temme, K.; Bravyi, S.; Gambetta, J. M. Error Mitigation for Short-Depth Quantum Circuits. *Phys. Rev. Lett.* **2017**, *119*, 180509.
(60) Li, Y.; Benjamin, S. C. Efficient Variational Quantum Simulator Incorporating Active Error Minimization. *Phys. Rev. X* **2017**, *7*, No. 021050.
(61) Giurgica-Tiron, T.; Hindy, Y.; LaRose, R.; Mari, A.; Zeng, W. J. Digital zero noise extrapolation for quantum error mitigation. *2020 IEEE International Conference on Quantum Computing and Engineering (QCE)* **2020**, 306−316.
(62) Yu, H.; Zhao, Y.; Wei, T.-C. Simulating large-size quantum spin chains on cloud-based superconducting quantum computers. *Phys. Rev. Res.* **2023**, *5*, No. 013183.
(63) Shao, Y.; Wei, F.; Cheng, S.; Liu, Z. Simulating Quantum Mean Values in Noisy Variational Quantum Algorithms: A Polynomial-Scale Approach. *arXiv:2306.05804v2* **2023**, DOI: 10.48550/arXiv.2306.05804.
(64) Nielsen, M.; Chuang, I. *Quantum Computation and Quantum Information: 10th Anniversary ed.*; Cambridge University Press, 2010.
(65) *Qiskit contributors Qiskit: An Open-source Framework for Quantum Computing*; ZENODO, 2023.
(66) Flick, J.; Schäfer, C.; Ruggenthaler, M.; Appel, H.; Rubio, A. Ab Initio Optimized Effective Potentials for Real Molecules in Optical Cavities: Photon Contributions to the Molecular Ground State. *ACS Photonics* **2018**, *5*, 992−1005.
(67) Ollitrault, P. J.; Kandala, A.; Chen, C.-F.; Barkoutsos, P. K.; Mezzacapo, A.; Pistoia, M.; Sheldon, S.; Woerner, S.; Gambetta, J. M.; Tavernelli, I. Quantum Equation of Motion for Computing Molecular Excitation Energies on a Noisy Quantum Processor. *Phys. Rev. Res.* **2020**, *2*, No. 043140.
(68) Pavošević, F.; Tavernelli, I.; Rubio, A. Spin-Flip Unitary Coupled Cluster Method: Toward Accurate Description of Strong Electron Correlation on Quantum Computers. *J. Phys. Chem. Lett.* **2023**, *14*, 7876−7882.

https://doi.org/10.1021/acs.jpclett.3c02875
J. Phys. Chem. Lett. 2024, 15, 1373−1381